Machine learning-based prediction and optimization of plasma-based conversion of CO_2 and CH_4 in an atmospheric pressure glow discharge plasma

Jiayin Li[1, 2, *], Jing Xu[3], Evgeny Rebrov[4, 5], Bart Wanten[1], and Annemie Bogaerts[1, 2, *]

[1] Research Group PLASMANT, University of Antwerp, Department of Chemistry, Antwerp, 2610, Belgium

[2] Electrification Institute, University of Antwerp, Olieweg 97, 2020 Antwerp, Belgium.

[3] School of Electronic Information and Communications, Huazhong University of Science and Technology, Wuhan, Hubei, 430074, People's Republic of China

[4] School of Engineering, University of Warwick, Coventry, CV4 7AL, the United Kingdom

[5] Department of Chemical Engineering and Chemistry, Eindhoven University of Technology, P.O. Box 513, 5600 MB Eindhoven, the Netherlands

[*] Corresponding author: jiayin.li@uantwerpen.be (J. Li), annemie.bogaerts@uantwerpen.be (A. Bogaerts).

Abstract

We developed a uniform, hybrid machine learning (ML) model, integrating both supervised learning (SL) and reinforcement learning (RL), based on several datasets across different CO_2 and CH_4 conversion reactions in an atmospheric pressure glow discharge plasma, to advance plasma-based CO_2 and CH_4 conversion. Given its complex and dynamic characteristics, the SL model employs artificial neural networks to predict performance, demonstrating excellent alignment with the entire experimental data. The RL model subsequently provides the optimization protocol, which prioritizes coarse adjustments to high-impact parameters then fine-tuning low-impact ones, to obtain the best performance. Furthermore, we also investigated the simultaneous optimization of the syngas ratio (SR) and energy cost (EC), resulting in a maximum SR of 2.12, combined with a minimum EC (syngas) of 2.04 eV/molec (i.e., 352 kJ/mol), which is close to the best experimental data obtained for further methanol synthesis, when accounting for suitable weight between SR and EC in the model. Our study emphasizes the importance of interpreting ML results based on prior knowledge and human analysis. We hope this work encourages a more critical view on the application of ML when studying plasma-based gas conversion.

Keywords

Plasma-based CO_2 and CH_4 conversion, Atmospheric pressure glow discharge, Machine learning, Process optimization, Syngas production

1. Introduction

Carbon dioxide (CO_2) and methane (CH_4) are the two major greenhouse gasses that significantly contribute to climate change.[1] Currently, there is an urgent need for the conversion of CO_2 and CH_4 into value-added chemicals or fuels.[2,3] The basic reaction is known as the dry reforming of methane (DRM), yielding valuable syngas (i.e., CO and H_2, theoretically in a 1:1 ratio), as shown in Eq. (1).

$$CH_4 + CO_2 \rightarrow 2CO + 2H_2, \ \Delta H_0 = 247.3 \ \text{kJ/mol} \quad (1)$$

Syngas is an important mixture of reactants to produce small organic compounds, which depend on the syngas ratio (SR, i.e., H_2/CO ratio).[4,5] For example, a SR of 2 is optimal for the Fischer − Tropsch process to create carbon-neutral fuels and lubricants when using a cobalt catalyst,[6] while a SR of around 1 is also suitable when using an iron catalyst,[7] but in general the optimal SR can vary between 1.7 and 2.15.[8] Also, a SR of 2 is considered as optimal for producing methanol, which facilitates a "methanol economy[9]" due to its higher energy density (compared to H_2), to be used in polymer chemistry and direct methanol fuel cells.[9,10]

Many technologies are being investigated for CO_2 and CH_4 conversion.[11,12] One of the innovative technologies gaining increasing attention, is plasma technology. Plasma is a (partially) ionized gas, and the electrons can generate various reactive species, such as atoms, ions, radicals, and molecules in both vibrational and electronic excited states. This reactive chemical cocktail allows to activate and dissociate stable gas molecules like CO_2 and CH_4 at mild temperature and pressure.[13] Furthermore, plasma is generated with electricity, and can be immediately switched on and off, thus enabling its integration with the fluctuating nature of renewable energy sources. Indeed, a recent techno-economic analysis demonstrated that the energy cost (EC) of plasma-based CO_2 conversion is 43% less than for electrolysis and conventional CO_2 conversion methods, achieving additional CO production from O_2 and enhanced CO_2 conversion by using a post-plasma carbon bed.[14]

Various plasma types have been studied for DRM.[8,15–22] To be competitive with traditional technologies, the EC should be below the threshold of 4.3 eV/molec, defined by Snoeckx and Bogaerts.[11] To achieve this, warm plasmas, like gliding arc, microwave, spark discharge and atmospheric pressure glow discharge (APGD), have shown promising results. Wanten et al. used a confined APGD (cAPGD) plasma reactor for DRM, and were able to convert 64% of CO_2 and 94% of CH_4, at an EC of 3.5 - 4 eV/molec, but they reached an SR of only 0.2 - 0.7.[23] To further reduce the EC, Maerivoet et al. investigated oxidative CO_2 reforming of methane (OCRM) in the same cAPGD, and reported that O_2 addition to the CO_2/CH_4 mixture could even reach a lower EC of 2 eV/molec.[24] However, the SR was still limited to ca. 0.8, making it difficult to produce methanol from syngas. To increase the SR, H_2O addition could act as additional source for H_2.[25] Therefore, Wanten et al. also investigated so-called bi-reforming of methane (BRM) in the cAPGD, and found that adding H_2O to the CO_2/CH_4 mixture increases the SR to 2, although it negatively affects the EC, reaching a minimum value of 3.9 eV/molec.[26] Therefore, combining an optimal SR with low EC in APGD plasma reactors is really challenging, due to the many interacting parameters, inherent to the complexity of plasma-based gas conversion systems.

To overcome these challenges, machine learning (ML) methods present a novel tool to efficiently investigate complex scientific phenomena.[27] Generally, ML can be mainly divided into several categories: a supervised learning (SL) model establishes a relationship between the input parameters and the desired output performance for static prediction, while a reinforcement learning (RL) model is a goal-oriented method, which

involves a decision-making process, by mapping actions for dynamic optimization. An unsupervised learning (UL) model involves training models on unlabeled data to discover hidden patterns, while a self-supervised learning model is a subset of UL, where labels are automatically generated from the data itself, enabling models to learn robust representations. These methods are gaining significant traction across diverse applications, including in plasma medicine,[28–30] chemical synthesis,[31-34] emissions control[35] and they also started to become applied in plasma-based gas conversion, specifically in dielectric barrier discharge (DBD) plasmas.[36–40] For instance, Liu et al. accurately predicted the reaction performance in plasma-based CH_4 conversion to hydrocarbons by using an artificial neural network (ANN) model,[36] while Zhu et al. investigated how various operating parameters affect the performance of CH_3OH oxidation.[37] Similarly, Wang et al. revealed a relationship between process parameters and performance targets in plasma-based DRM to oxygenates.[38] Recently, Cai et al. developed a hybrid SL model to identify the optimal conditions for maximum energy efficiency in plasma-catalytic DRM.[39] We went one step further, and developed the very first RL model for process optimization of plasma-catalytic DRM.[40] The reason that all these ML approaches were applied to DBD plasmas is because of the much larger datasets available. However, DBD plasmas exhibit limited performance compared to so-called warm plasmas; for instance, their EC is often excessively high.[41,42]

Optimization of the operating conditions of plasma-based CO_2 and CH_4 conversion typically leads to trade-offs among conflicting objectives (e.g., higher conversion vs. higher SR vs. higher energy efficiency[11,23,24,26]) and traditional trial-and-error efforts might have reached their limit. To achieve a cost-effective plasma-based gas conversion system with optimal reaction performance, a thorough understanding is needed on how the interconnected operating parameters can be dynamically optimized. To our knowledge, no studies have considered the prediction and optimization of plasma-based CO_2 and CH_4 conversion in warm plasmas, such as an APGD, by means of a ML method. Typically, optimizing the chemical performance using a ML approach requires a consistent, relevant, and sufficient amount of data for accurate prediction. However, there is limited experimental data for warm plasmas (like APGD) in each separate study. Moreover, experimental data from different groups cannot be directly compared, as they are evaluated under different reaction conditions using different setups.[43] Therefore, developing a uniform ML model for warm plasmas (such as an APGD) may be challenging, due to the lack of available datasets.

In previous work, the PLASMANT group investigated in detail DRM,[23] OCRM[24] and BRM[26] in a cAPGD plasma reactor. These three reactions are important for the simultaneous CO_2 and CH_4 conversion, and the O_2 and H_2O addition (i.e., OCRM and BRM, respectively) help to improve the performance, as explained above. Hence, they can be considered as two extra input parameters in a ML model development, thus enlarging the size of the available dataset. Moreover, the latter allows us to test the applicability of ML across widely varying datasets. In addition, the reactor design for the DRM, OCRM and BRM reaction was the same, although a slightly upgraded version of the reactor was used for BRM, by using a movable cathode to allow lower ignition voltages. Changing the interelectrode distance changes the residence time of

the molecules in the plasma, but this was found to have no impact on the performance when comparing with the fixed cathode case (i.e., the APGD reactor used in DRM and OCRM) within a sufficiently wide range. Therefore, the data collected in BRM, together with the DRM and OCRM reactions, can be used for developing a consistent ML model. Compared with an SL model, an RL model is more suitable for simultaneous multi-objectives optimization, through its dynamic and interactive learning capabilities.

In the present work, we therefore design a uniform, hybrid ML (SL+RL) model for both prediction and optimization of plasma-based conversion of CO_2 and CH_4 in a cAPGD reactor, especially aiming to increase the SR, making it useful for further methanol production. Specifically, we developed the SL (prediction) model for the reaction performance (i.e., CO_2 and CH_4 conversion, H_2 and CO yield, SR, and EC) by using an artificial neural network (ANN) algorithm. Furthermore, we designed an RL model to simultaneously maximize the SR and minimize the EC, by using the SL model as a simulation environment for learning interactions. This work provides new insights into multi-objectives optimization in warm plasma reactors for gas conversion applications.

2. Methodology

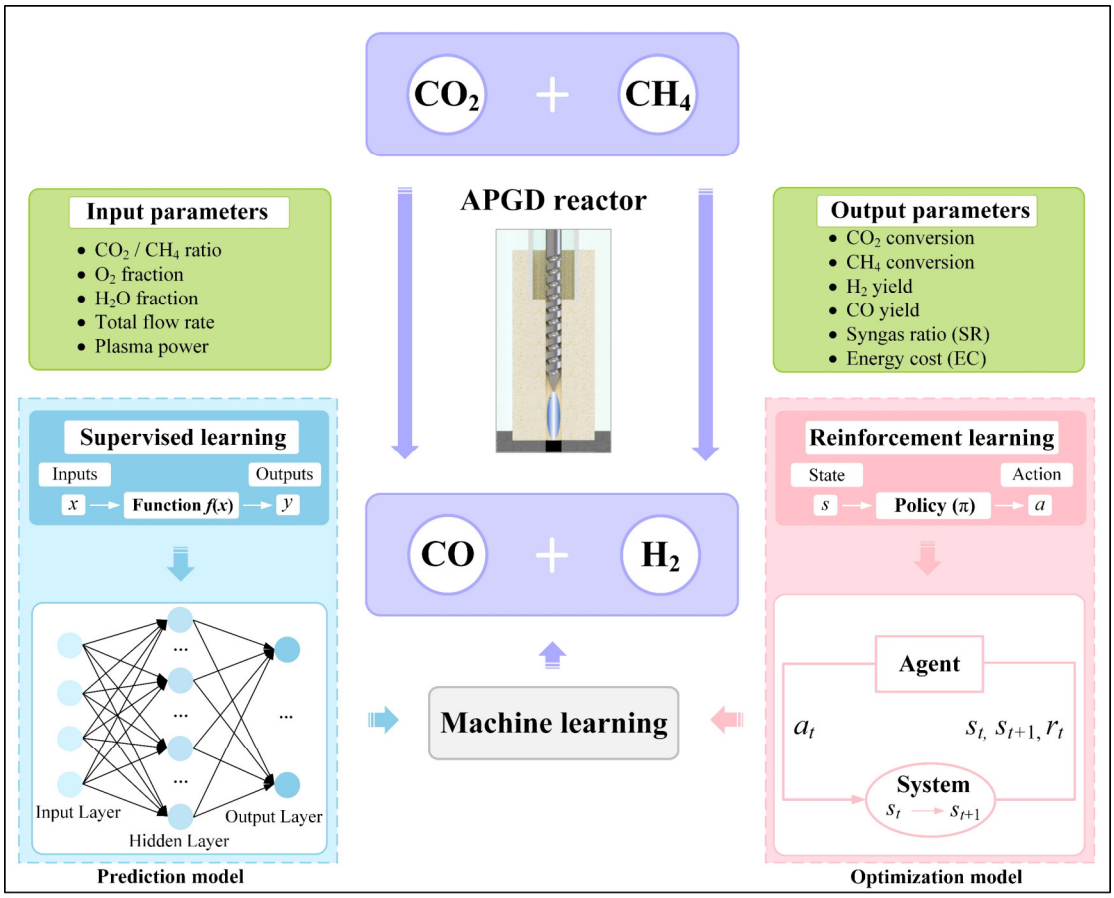

Fig.1 Overview of the ML model for plasma-based CO_2 and CH_4 conversion in an APGD reactor. The SL (prediction) model acquires a function $f(x)$, mapping inputs x to outputs y, while the RL (optimization) model involves mapping states to actions, based on policy (π). Abbrev: a_t (action), r_t (reward), s_t and s_{t+1} (state).

In this work, we used two ML methods, i.e., SL and RL, to develop a model for plasma-based conversion of CO_2 and CH_4 in an APGD reactor, as schematically illustrated in Figure 1, and elaborated in detail in the subsequent sections. All abbreviations relevant for these methods can be found in the Supporting Information (SI, section 1, Table S1).

2.1 Data collection and processing

Fig. S1 in the SI (section 2) shows the experimental setup of the cAPGD reactor for CO_2 and CH_4 conversion, which is described in detail in.[23,24,26] By varying the input parameters, including the CO_2/CH_4 ratio, O_2 fraction, H_2O fraction, total flow rate and plasma power, the output parameters, i.e., CO_2 conversion, CH_4 conversion, CO yield, H_2 yield, SR and EC, were collected as the dataset. To allow a fair investigation among the DRM, OCRM and BRM reactions, the EC was expressed in eV/molec syngas produced (i.e. CO and H_2 combined, with the SR under the corresponding conditions), because syngas serves as the product shared among all reactions. We investigated 84 distinct reaction conditions to cover the key metrics of the reaction performance, and also to ensure stable and reliable plasma conditions. The collected data, listed in Tables S1 and S2, were used for training the ML model. Before the model development, all datasets were pre-processed by a Min-Max normalization method. The complete dataset was divided into a 75% training subset and a 25 % testing subset.

To mitigate risks of overfitting and enhance the model's generalizability beyond the training data, we adopted 5-fold cross-validation method due to the limited size of the dataset. This technique involves randomly dividing the data into five distinct subsets, iteratively training the model on four subsets and testing (validating) it on the fifth. Each subset serves as the test (validation) set exactly once across the five iterations, ensuring evaluation of performance consistency.

2.2 Description of the SL model: artificial neural network (ANN)

ANN, a well-established SL algorithm, was employed to predict the performance of plasma-based conversion of CO_2 and CH_4 across diverse operating conditions, leveraging their demonstrated capacity to model complex non-linear relationships.[38] The ANN architecture comprises interconnected artificial neurons with adjustable weights, which act as learnable parameters to drive the model's training. Generally, the model consists of multiple layers, where each node encodes specific features of the input-output relationships. In this study, a fully connected architecture was adopted. The five predefined operating parameters served as inputs, while the six target performance metrics were designated as outputs.

To refine the neural network parameters, we employed the backpropagation (BP) algorithm, leveraging gradient descent, as indicated in Ref.[44] The ReLU activation function was employed to address complex nonlinear relationships and mitigate gradient vanishing issues. For loss computation, the mean squared error (MSE) metric was selected to enhance the efficiency of gradient descent, promoting rapid convergence and stability in regression tasks. Furthermore, model performance was rigorously assessed using two complementary metrics: MSE, which quantifies prediction error magnitude, and the coefficient of determination (R^2), which evaluates

the proportion of variance explained by the model. These metrics were calculated for both training and testing phases to ensure robustness and generalizability:[45]

$$MSE = \frac{1}{n}\sum_{i=1}^{n}(y_i - \hat{y}_i)^2 \tag{2}$$

$$R^2 = 1 - \frac{\sum_{i=1}^{n}(y_i - \hat{y}_i)^2}{\sum_{i=1}^{n}(y_i - \overline{y})^2} \tag{3}$$

where y_i is the actual value, $\hat{y}_i$ is the predicted value and $\overline{y}$ is the mean of the actual value. In general, achieving high model accuracy typically requires maximizing R^2 and minimizing MSE.[46] To optimize the ANN model, we utilized a grid search strategy for hyperparameter tuning—a method well-suited for systematically exploring complex parameter spaces in multi-layered architectures.[47] After identifying the optimal hyperparameters (see MSE trends illustrated in Fig. S2), the finalized ANN configuration is detailed in Table 1.

Table 1. Detailed parameters of the ANN model

Parameter	ANN model
Number of input layers	5
Number of hidden layer 1	90
Number of hidden layer 2	55
Number of hidden layer 3	35
Number of hidden layer 4	41
Number of output layers	6
Activation function	ReLU
Optimizer	lbfgs
Loss function	MSE
Evaluation indicator	MSE and R^2

2.3 Algorithm comparison

To identify the optimal predictive model, two other ML algorithms, namely support vector regression (SVR) and regression trees (RT), were selected for comparison. SVR, a robust methodology for nonlinear regression, constructs hyperplanes in high-dimensional feature spaces, offering distinct advantages for scenarios involving limited sample sizes, nonlinear relationships, or complex dimensionality. The RT model, another classical supervised regression algorithm, operates by iteratively partitioning the dataset through feature-based splits, guided by statistical significance, until predefined termination conditions are satisfied. The hyperparameters of the models are shown in Table. S4.

2.4 Methods of significance analysis

The linear relationships between input variables were assessed using Pearson's Correlation Coefficient (PCC), a metric ranging from -1 (indicating a negative

correlation) to +1 (indicating a positive correlation). The PCC is defined as: [48,49]

$$\rho_{xy} = \frac{\Sigma(x_i - x_{mean})\,(y_i - y_{mean})}{\sqrt{\Sigma(x_i - x_{mean})^2 \Sigma(y_i - y_{mean})^2}} \quad (4)$$

where ρ_{xy} represents the PCC value between the input feature and output target, x_{mean} indicates the averages of input feature x and y_{mean} indicates the averages of output target y, respectively. By analyzing the magnitude of the PCC values (i.e., their absolute values), the relative importance of the five operating parameters on chemical performance was evaluated.

2.5 Description of the RL model: Proximal Policy Optimization (PPO)

SL methods learn to predict patterns, but they do not inherently execute actions or make decisions. In contrast, RL models learn an optimal decision policy by actively interacting with a dynamic environment to maximize the desired outcomes. Indeed, the RL model can be treated as a feedback-driven system where the learner's actions directly shape subsequent environmental states, as shown in Fig.1.[50] Within this paradigm, the *agent* (the learning entity) interacts with the *environment* (the external system), observing the state of environment (s_t), choosing an action $a(t)$ to reach a new state (s_{t+1}), and receiving rewards $r(t)$ that evaluates the action's efficacy. These rewards guide the agent's behavior, enabling it to iteratively refine its policy, $\pi(a|s)$, to maximize long-term rewards.

In this work, we designed such RL agents, to identify the optimal SR and minimum EC by dynamically adjusting five operational parameters. The agent was trained by the PPO algorithm built on the AC framework (see Fig. S3), which performs effectively within the continuous data space.[51] More details could be found in our previous work.[40] By employing trajectory visualization techniques, we analyzed the agent's decision-making process to derive optimal performance regulation strategies. The detailed parameters of the RL model are listed in Table S5.

3. Results

3.1 SL models evaluation

We first calculated the R^2 and MSE values for the training and test datasets separately, to check for overfitting, as shown in Table 2 and Table 3. The average R^2 of the SL models in the training dataset were found to be 0.99074 for ANN, 0.992938 for RT and 0.975533 for SVR, respectively. The average R^2 of the SL models in the test dataset were found to be 0.976285 for ANN, 0.870211 for RT and 0.944651 for SVR, respectively. For MSE, its average values in the training dataset were identified as 0.0005765 for ANN, 0.001974 for RT and 0.001522 for SVR, respectively. In the test dataset, its average values were identified as 0.002304 for ANN, 0.008738 for RT and 0.003072 for SVR, respectively. The R_2 and MSE values in the training dataset are very close to those in the test dataset so the SL models are not overfitting. On the other hand, the performance of these three algorithm models followed the order ANN > SVR > RT, the ANN model was then chosen as the SL algorithm for the prediction model.

The ANN model's performance is evaluated by comparing its predicted values with

the actual (experimental) values for the performance (conversion, yield, SR and EC), as shown in Fig. 2 and Fig. 3. The ANN prediction model shows very good accuracy through the entire dataset, achieving an R^2 consistently higher than 0.96. This demonstrates that the ANN model is able to predict the plasma-based conversion of CO_2 and CH_4, providing a robust basis for further developing the RL model. To further validate the ANN model's generalizability, i.e., the robustness and adaptability of the model, we performed additional experiments using new operating parameters within the investigated ranges (CO_2/CH_4 ratio = 1.9, H_2O fraction = 0%, plasma power = 89 W, total flow rate = 1 L/min and O_2 fraction = 0 - 15%). As presented in Fig. S4, the model's predictions on unseen data align well with the actual (experimental) data, thereby confirming its reliability.

Table 2. R^2 values for the training and test dataset

R^2 of Dataset	Model	CO_2 conversion	CH_4 conversion	CO yield	H_2 yield	Syngas ratio	Energy cost
Training dataset	ANN	0.991935	0.994513	0.985646	0.986781	0.998768	0.986781
	RT	0.993787	0.998650	0.999061	0.988424	0.996950	0.980756
	SVR	0.966463	0.972702	0.965130	0.954324	0.999210	0.995366
Test dataset	ANN	0.961925	0.955161	0.975608	0.983460	0.998026	0.983534
	RT	0.819299	0.758787	0.829638	0.911105	0.982471	0.919968
	SVR	0.921932	0.919021	0.900590	0.949489	0.997871	0.979004

Table 3. MSE values for the training and test dataset

MSE of Dataset	Model	CO_2 conversion	CH_4 conversion	CO yield	H_2 yield	Syngas ratio	Energy cost
Training dataset	ANN	0.000413	0.000187	0.000487	0.000477	0.000336	0.001559
	RT	0.000296	0.000064	0.000047	0.000462	0.000833	0.010143
	SVR	0.001600	0.001297	0.001757	0.001822	0.000216	0.002442
Test dataset	ANN	0.002189	0.002203	0.002101	0.002215	0.000506	0.004607
	RT	0.007287	0.006979	0.007470	0.003807	0.004496	0.022393
	SVR	0.003148	0.002343	0.004359	0.002163	0.000546	0.005875

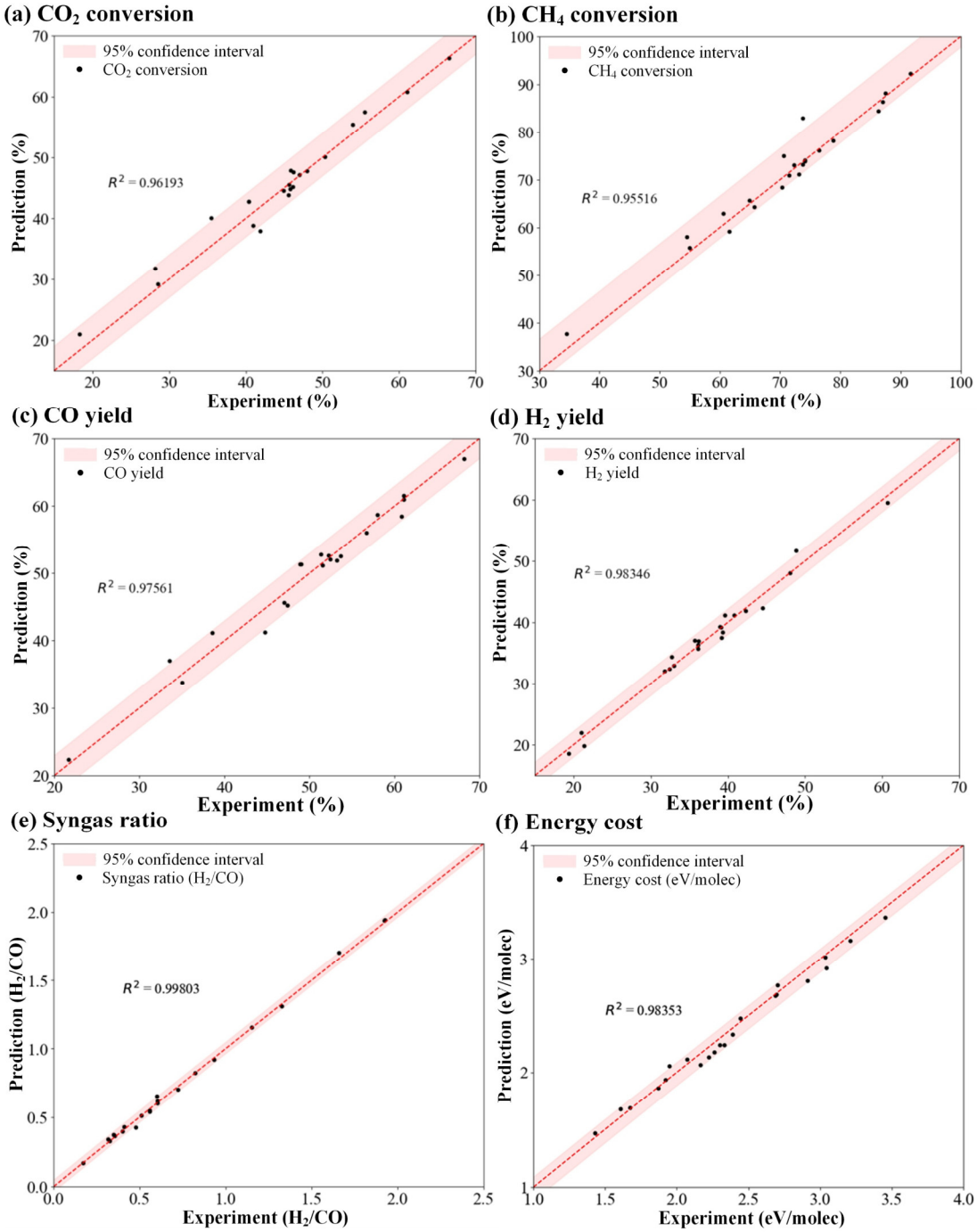

Fig. 2. Predicted data versus experimental results (R^2 plot). (a) CO_2 conversion; (b) CH_4 conversion; (c) CO yield; (d) H_2 yield; (e) syngas ratio and (f) energy cost.

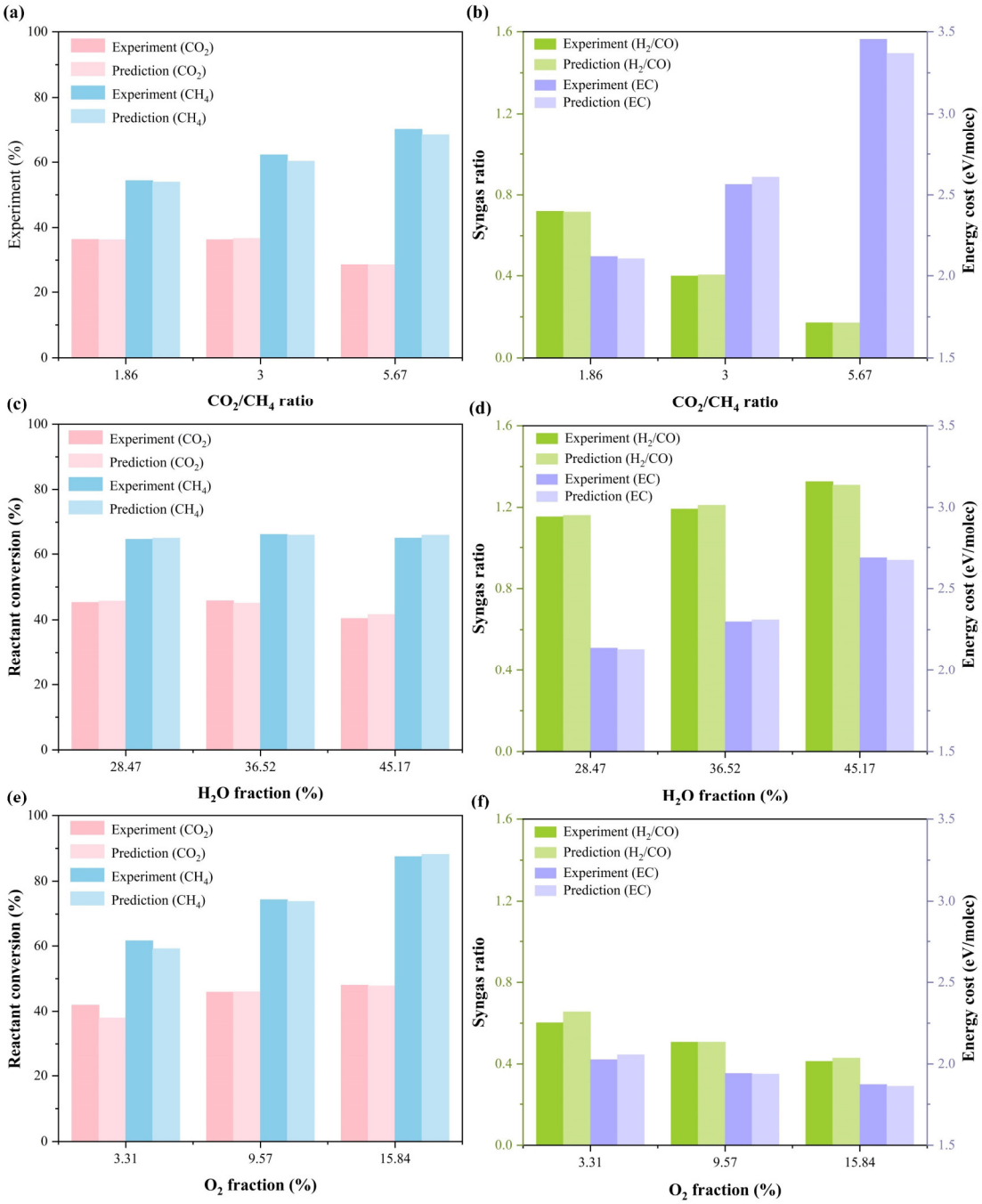

Fig.3. Comparison of predicted values with available experimental data of plasma-based CO_2 and CH_4 conversion. (a) and (b) CO_2/CH_4 ratio (plasma power = 96 W, total flow rate = 1 L/min, O_2 and H_2O fraction = 0%); (c) and (d) H_2O fraction (plasma power = 300 W, total flow rate = 3 L/min, CO_2/CH_4 ratio = 1, O_2 fraction = 0%); (e) and (f) O_2 fraction (plasma power = 96 W, total flow rate = 1 L/min, CO_2/CH_4 ratio = 1.9, H_2O fraction = 0%).

3.2 Relative importance of the input parameters, and relationship with the output parameters

The relative importance of each input parameter and the correlation between operating parameters and performance parameters are demonstrated in Fig. 4 and Table 4. The most important input parameter is the total flow rate, at least for CO_2 conversion

(50.1 %), CH_4 conversion (40.1%) and CO yield (39.6%). Furthermore, the O_2 fraction is the most important parameter for EC (45.8%), while the H_2O fraction mostly influences the SR (26.9%), and the CO_2/CH_4 ratio mostly affects the H_2 yield (53.7%). Finally, the plasma power has only minor impact on all performance parameters, except for the SR. These results will be discussed in section 4 below.

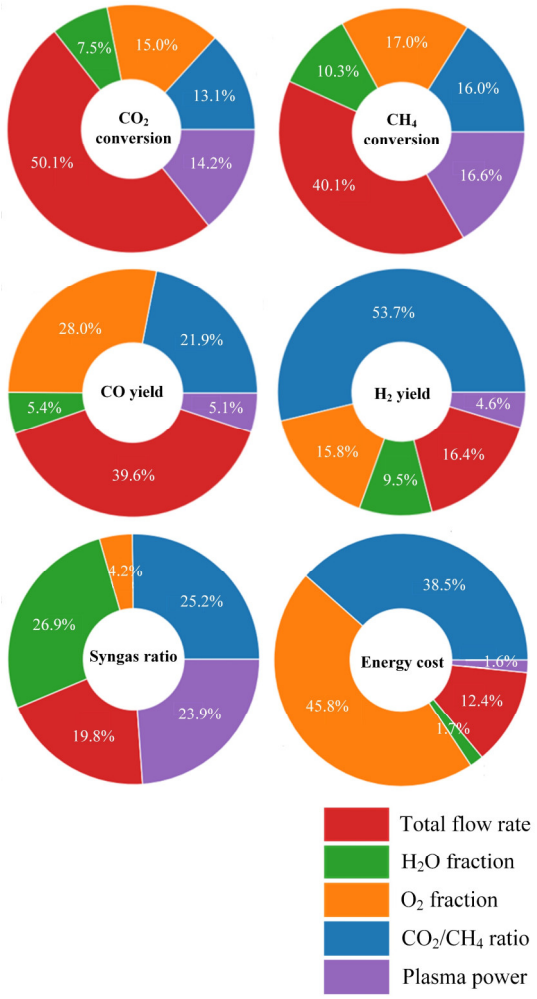

Fig. 4. Relative importance of the five different operating parameters for determining the CO_2 and CH_4 conversion, CO and H_2 yield, SR and EC.

Table 4. Relative importance of the different input parameters for determining the various output parameters

Output	1st IF	2nd IF	3rd IF	4th IF
CO_2 conversion	Flow (50.1%) (-)	O_2 frac. (15.0%) (+)	Power (14.2%) (+)	Ratio (13.1%) (↗ ↘)
CH_4 conversion	Flow (40.1%) (-)	O_2 frac. (17.0%) (+)	Power (16.6%) (+)	Ratio (16.0%) (+)
CO yield	Flow (39.6%) (-)	O_2 frac. (28.0%) (+)	Ratio (21.9%) (+)	H_2O frac. (5.4%) (-)
H_2 yield	Ratio (53.7%) (-)	Flow (16.4%) (-)	O_2 frac. (15.8%) (-)	H_2O frac. (9.5%) (-)
Syngas ratio	H_2O frac. (26.9%)	Ratio (25.2%)	Power (23.9%)	Flow (19.8%)

	(+)	(-)	(-)	(↗↘)
Energy cost	O_2 frac. (45.8%)	Ratio (38.5%)	Flow. (12.4%)	H_2O frac. (1.7%)
	(−)	(+)	(+)	(+)

Abbreviations used in the table: Important factor (IF), O_2 fraction (O_2 frac.), H_2O fraction (H_2O frac.), CO_2/CH_4 ratio (Ratio), total flow rate (Flow) and plasma power (Power). Positive factor and negative factor are represented by (+) and (-), respectively. When the output parameter first increases and then decreases with rising input parameters, it is indicated as (↗↘).

3.3 RL model evaluation

The investigated range of the five input parameters is as follows: CO_2/CH_4 ratio (0.33 - 5.67), O_2 fraction (0 - 15%), H_2O fraction (0 - 45%), Power (71.7 - 400.4 W) and total flow rate (0.5 - 3 L/min). The typical RL agent training results are shown in Fig. S5 of the SI. All RL calculations (i.e., to obtain the optimal performance corresponding with the actions of agents) were performed within the investigated range.

Fig. 5 presents the testing curve of the RL models for CO_2 and CH_4 conversion, including their corresponding actions within the range of input parameters. The latter represents how the input parameters affect the evolution of the CO_2 and CH_4 conversion towards their optimal values. Fig. 5 (a) and Fig. 5 (b) illustrate that the CO_2 conversion can reach its maximum value of 75.7% when the total flow rate first reaches its lower boundary (i.e. 0.5 L/min), and then the plasma power reaches its upper boundary (i.e. 400.4 W), followed by the O_2 fraction reaching its upper boundary (i.e. 15%). It is interesting to note that the CO_2/CH_4 ratio first increases and then decreases to an optimal value (the reason will be further discussed in section 4.2).

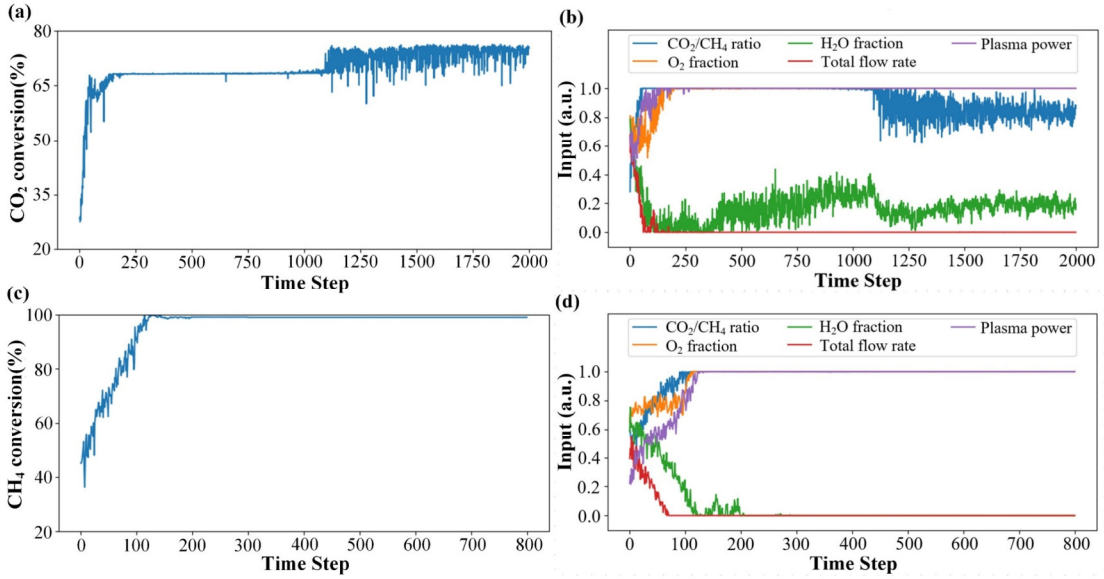

Fig. 5. Testing curve of the RL models for (a) CO_2 conversion and (c) CH_4 conversion, by plotting them against time step, as well as the corresponding actions (b) and (d). The y-axis representing the input parameters (for (b) and (d)) shows the normalized values, with 0 and 1 being the lower and upper boundary, respectively.

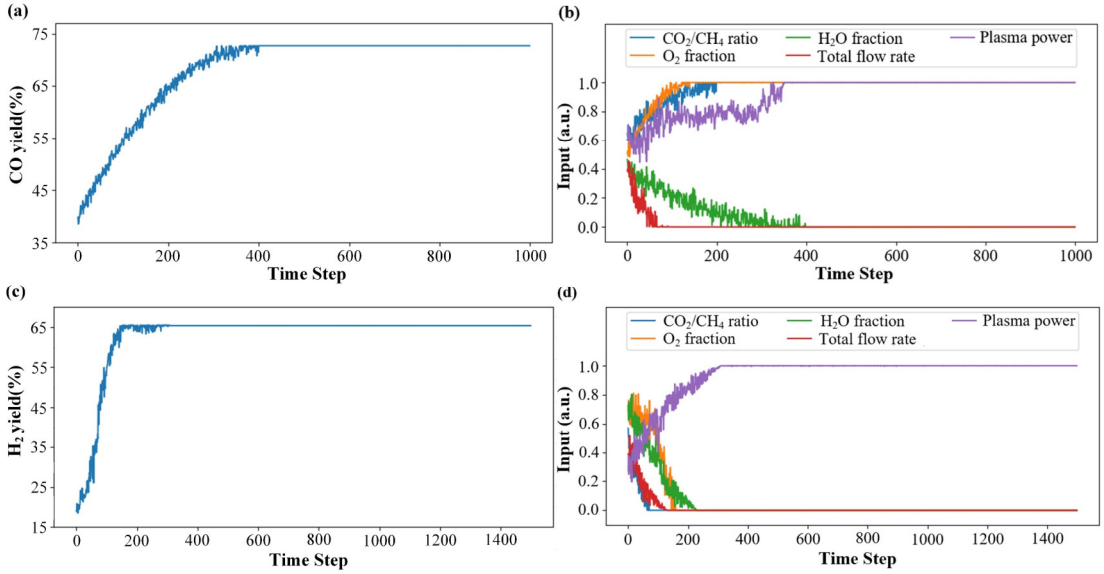

Fig. 6. Testing curve of the RL models for (a) CO yield and (c) H_2 yield, by plotting them as a function of time step, as well as the corresponding actions (b) and (d). The y-axis representing the input parameters (for (b) and (d)) shows the normalized values, with 0 and 1 being the lower and upper boundary, respectively.

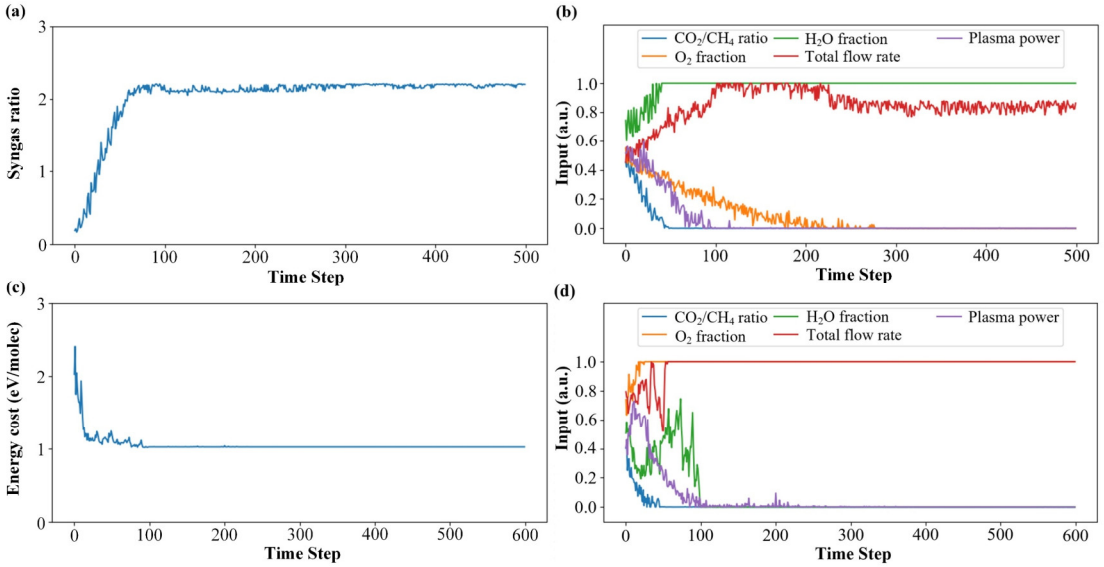

Fig. 7. Testing curve of the RL models for (a) syngas ratio and (c) energy cost, by plotting them as a function of time step, as well as the corresponding actions (b) and (d). The y-axis representing the input parameters (for (b) and (d)) shows the normalized values, with 0 and 1 being the lower and upper boundary, respectively.

On the other hand, the CH_4 conversion can reach its maximum value of 98 % when the total flow rate first reaches its lower boundary (i.e. 0.5 L/min), followed by the CO_2/CH_4 ratio and O_2 fraction reaching their upper boundary (i.e. 5.67 and 15%). As is clear from the relative importance in Table 4, the most important factor for the CO_2 and CH_4 conversion is the total flow rate, so the agent first optimizes this parameter. Because the relative importance of plasma power (14.2%) and O_2 fraction (15.0%) is very close to each other for the CO_2 conversion, the agent optimizes them as the

following (second and third) parameters. The optimal policy with factors of similar relative importance (plasma power, O_2 fraction and CO_2/CH_4 ratio) is also applied to the CH_4 conversion.

A similar regulation policy can be found in Fig. 6, which presents the time step-dependence of the CO and H_2 yield, with the corresponding actions. Fig. 6 (a) show that the CO yield can reach its maximum value of 71 % when the total flow rate first reaches its lower boundary (i.e. 0.5 L/min), followed by the O_2 fraction and CO_2/CH_4 ratio reaching their upper boundary (i.e. 15% and 5.67) (Fig. 6 (b)), respectively. On the other hand, the H_2 yield can reach its maximum value of 65% when the CO_2/CH_4 ratio first reaches its lower boundary (i.e. 0.33), followed by the total flow rate and O_2 fraction reaching their lower boundary (i.e. 0.5 L/min and 0%) (Fig. 6 (d)). The two less important factors, i.e. plasma power and H_2O fraction can reach their upper boundary and lower boundary (i.e. 400.4W and 0%), respectively.

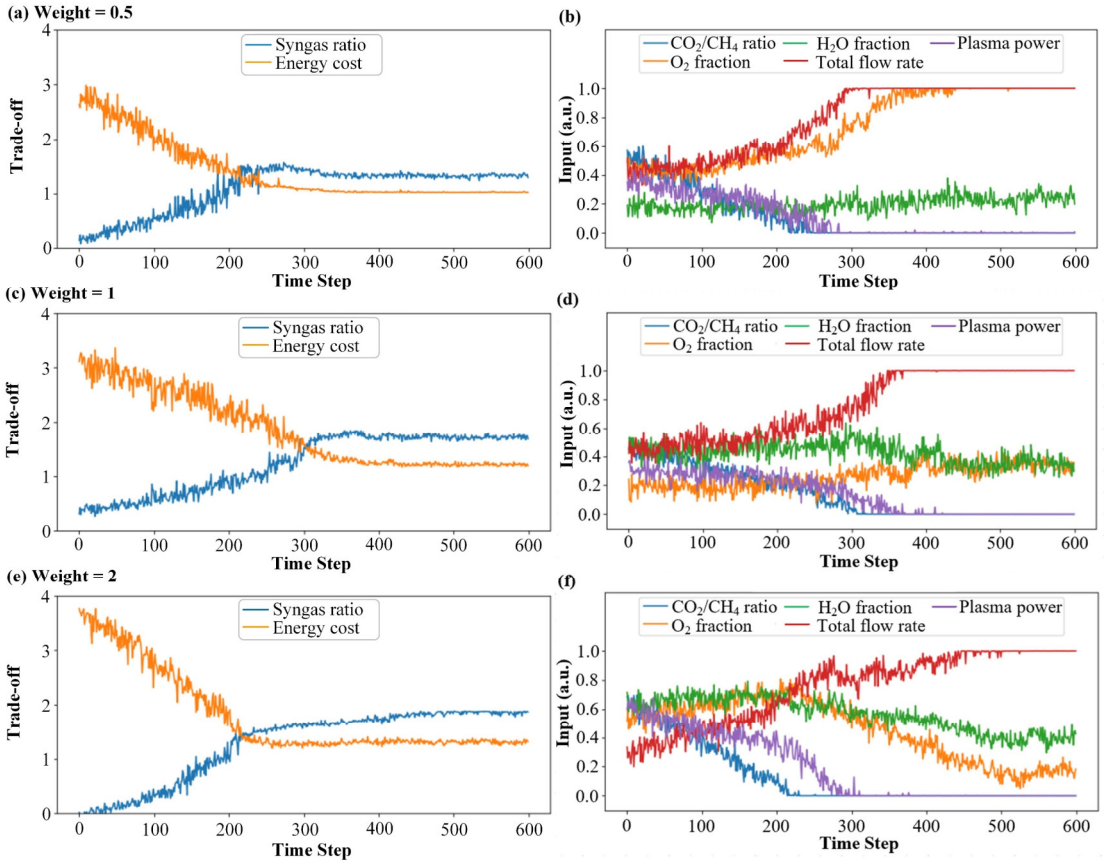

Fig. 8. Superposition of syngas ratio and energy cost, showing the best trade-offs (a, c, e), as well as the corresponding actions of the five input parameters (b, d, f), for different weights, i.e., relative importance of SR vs EC: weight = 0.5 (a) and (b), weight = 1 (c) and (d), weight = 2 (e) and (f).

The testing curve of the RL models for the SR and EC, with the corresponding actions, is presented in Fig. 7. From Fig. 7 (a) and Fig. 7 (b), we can see that the SR can reach its maximum value of 2.2 when the H_2O fraction first reaches its upper boundary (i.e. 45%), followed by the CO_2/CH_4 ratio reaching its lower boundary (i.e. 0.33), while the O_2 fraction is the last to reach its lower boundary (i.e. 0%). The EC can reach its minimum value of 1 eV/molec when the O_2 fraction reaches its upper boundary (i.e. 15%), followed by the CO_2/CH_4 ratio reaching its lower boundary (i.e. 0.33). Note that

the H_2O and O_2 fraction yield a trade-off between SR and EC.

In addition to separately investigating the SR and EC, we need a comprehensive understanding of the effect of all operating parameters for optimizing both performance metrics of plasma-based CO_2 and CH_4 conversion. To account for the practical need in applications, we present in Fig. 8 the superposition of SR and EC for different weights (i.e., relative importance of SR vs EC, equal to 0.5, 1 and 2, as an example), with the corresponding actions. The convergence trends of SR and EC are similar, but their optimal values depend on the weights (for weight = 0.5, SR_{max} = 1.33 and EC_{min} =1.04 eV, for weight = 1, SR_{max} = 1.76 and EC_{min} =1.23 eV and for weight = 2, SR_{max} = 1.88 and EC_{min} =1.36 eV). Hence, at a higher weight of SR vs EC, a higher maximum SR and a higher minimum EC are reached, and vice versa, at a lower weight of SR vs EC, a lower maximum SR and a lower minimum EC are reached. With increasing weight, the optimal H_2O fraction increases, while the optimal O_2 fraction decreases, which corresponds with the results of the separate SR and EC optimization, and it is in line with our expectations, because the H_2O fraction is mainly important for optimizing the SR, while the O_2 fraction is more important for optimizing the EC. Moreover, the total flow rate can reach its upper boundary and the CO_2/CH_4 ratio can reach its lower boundary for the optimization of all weighted superpositions.

4. Discussion

4.1 Optimal policy developed by the RL model

Table 5. Regulation sequence of various input parameters within their range

Objectives	1st order	2nd order	3rd order	4th order
CO_2 conversion ↑	Flow (↓)	Power (↑)	O_2 frac. (↑)	Ratio (optimal)
CH_4 conversion ↑	Flow (↓)	Ratio (↑)	O_2 frac. (↑)	Power (↑)
CO yield ↑	Flow (↓)	O_2 frac. (↑)	Ratio (↑)	Power (↑)
H_2 yield ↑	Ratio (↓)	Flow (↓)	O_2 frac. (↓)	H_2O frac. (↓)
Syngas ratio ↑	H_2O frac. (↑)	Ratio (↓)	Power (↓)	Flow (optimal)
Energy cost ↓	O_2 frac. (↑)	Ratio (↓)	Flow (↑)	H_2O frac. (↓)

Abbreviations used in the table: O_2 fraction (O_2 frac.), H_2O fraction (H_2O frac.), CO_2/CH_4 ratio (Ratio), total flow rate (Flow) and plasma power (Power). When the factors reach their upper and lower bounds, it is represented by (↑) and (↓), respectively. The expected objective is to maximize the reaction performance and minimize the EC, which is represented by (↑) and (↓), respectively.

Through an analysis of the relative importance of input parameters in governing the output parameters (Table 4), we derived two optimization strategies, summarized in Table 5. First, the agent's actions on the input parameters correspond to their observed directional influence on the output parameters. To maximize the reaction performance, parameters with positive correlations reach their upper bounds, while parameters with negative correlations reach their lower bounds. Parameters exhibiting non-monotonic relationships (i.e., those where performance first increase (decrease) and then decrease (increase)) are optimized at intermediate values. To minimize the EC, the O_2 fraction should reach its upper bound and the H_2O fraction should reach its lower bound, since the EC decreases with increasing O_2 fraction and decreasing H_2O fraction. Second, the

RL model reveals the optimal policy (regulation sequence): the agent prioritizes coarse adjustments to high-impact parameters then fine-tuning low-impact ones, to obtain the maximum rewards, i.e., achieve the maximum reaction performance and minimum EC. Considering that the relative importance of some input parameters are very close to each other (their difference is lower than 1%), we can conclude that the regulation sequence exhibits good agreement with the predicted importance results. This indicates that the RL agent can make rational, human-like decisions when managing complex interactions among parameters.

4.2 Explanation of the effect of the various input parameters, for DRM, BRM and OCRM

Changing the CO_2/CH_4 input ratio has a different impact on CO_2 conversion in the DRM vs BRM reaction. In the absence of H_2O, the CO_2 conversion decreases with increasing CO_2/CH_4 ratio (pure DRM). However, in the presence of H_2O, the CO_2 conversion increases with increasing CO_2/CH_4 ratio (hence showing the opposite pattern for BRM). This interesting phenomenon can be explained by the water–gas shift (WGS) reaction and Le Chatelier's principle.[26] The WGS reaction acts as side reaction, for both DRM and BRM, i.e., $H_2O + CO \rightarrow H_2 + CO_2$, as reported in literature.[52,53] At high H_2O fraction (45 vol%) and very low CO_2 fraction (e.g. 14 vol% at the lowest CO_2/CH_4 input ratio), this side reaction is heavily promoted following Le Chatelier's principle, and it leads to less CO_2 and more H_2O being converted. The opposite is observed in case of only CO_2 and CH_4 and no H_2O in the input stream. Here, the CO_2 fraction in the mixture decreases from 85 to only 65 vol%, so it remains quite high, while the produced amount of H_2O is not that high. Together with the increased amount of H_2, produced from CH_4, the "reverse" WGS reaction will be promoted, leading to even more CO_2 conversion and H_2O production. It should be noted that the exact chemistry will be more complex than this simple reasoning, and changing temperature upon changing the CO_2/CH_4 ratio might also play a role.[53] However, the above simple reasoning can explain some of the observed trends.

In terms of yields and production rates, decreasing the CO_2/CH_4 ratio will reduce the CO yield and increase the H_2 yield, this is attributed to the enhanced conversion rate of CH_4 and H_2O, alongside the reduced CO_2 conversion rate at lower CO_2/CH_4 ratio.[26] On the other hand, the production rates of CO and H_2 increase with decreasing CO_2/CH_4 ratio. Therefore, the SR rises to 2.03 at CO_2:CH_4 ratio of 0.33, more than twice the value observed at a ratio of 1.86, which is the best result in our current dataset.

Overall, the H_2O fraction has a low impact (relative importance is lower than 11%) and it negatively affects the reactant conversions and product yields, which is also observed in other works.[52,54,55] However, it has a significant positive effect on the SR, which rises upon H_2O addition. In addition, the H_2O fraction obviously reduces the conversion rate for both CO_2 and CH_4, when these components are fed at lower flow rates.[26] The rate of H_2 production also declines, but as little because additional hydrogen is being produced from H_2O plasmolysis. In the RL model result, we can also observe that the CO_2/CH_4 ratio reaches its lower boundary (i.e., CO_2 input fraction is decreased). Based on the BRM reaction equation ($CO_2(g) + 2\ H_2O(l) + 3\ CH_4(g) \rightleftharpoons 4\ CO(g) + 8$

H_2(g)), the CH_4 fraction should indeed increase further, to achieve a SR reaching 2. Therefore, the addition of H_2O has been shown to be advantageous, particularly when the CO_2/CH_4 ratio is reduced at the same time. In addition, adding water helps enhance plasma stability in situations where excessive soot would otherwise be generated, which was confirmed by previous works.[54–57]

The O_2 fraction typically results in a more stable plasma because of the improved oxidation of solid carbon generated from CH_4 decomposition,[58] alongside a greater conversion of all reactants, but a less valuable product output (SR). The SR declines as the O_2 fraction rises, because the production of H_2O from CH_4 and O_2 limits the amount of available hydrogen necessary for H_2 production. It should also be noted that a lower CO_2/CH_4 input ratio, combined with a higher O_2 fraction, can reach a higher SR (but still lower than in the case of H_2O addition) but it may lead to unstable plasma conditions because of excess solid carbon formation.[24] Furthermore, as mentioned above, a higher O_2 fraction is beneficial for both CH_4 and CO_2 conversion. The enhanced CH_4 conversion with a higher O_2 fraction can be attributed to an additional exothermic reaction pathway besides DRM, i.e., the partial oxidation of CH_4 with O_2 and by a higher gas temperature, due to the energy released by the reaction of O_2 with CH_4. This higher gas temperature will also lead to a higher CO_2 conversion.[59]

4.3 Critical view on the ML results

Data-driven ML models can accurately learn from a complete dataset to identify complex trends. For instance, a higher CO_2/CH_4 ratio enhances the CO_2 conversion in the presence of H_2O (BRM reaction), while it reduces the CO_2 conversion in the absence of H_2O (DRM reaction), so it should have an optimal value, rather than an upper boundary or lower boundary across the entire dataset, to maximize the CO_2 conversion. We believe this observation, combined with Le Chatelier's principle described in section 4.2, is a logical explanation for the ML results.

However, ML can also lead to wrong results, due to the limited data, even though it may identify the correct trends. The total flow rate is the most important (negative) factor for the CO_2 and CH_4 conversion, as well as for the CO yield, based on the SL (ANN) prediction, which is in line with literature.[39] From a chemical perspective, this trend is attributed to a reduced residence time of the reactant gases in the discharge zone at an elevated total flow rate, which diminishes the chances of collisions between the reactants (CH_4 and CO_2) and active species, such as energetic electrons, excited species, and radicals (e.g., CHx, O, and H). This, in turn, leads to reduced CO_2 and CH_4 conversion, resulting in lower CO and H_2 yields. However, it should be noted that the training data set related to total flow rate is quite limited. Minor data changes can therefore lead to dramatic changes in the predictions of conversion, by the SL model. In other words, the fact that the total flow rate is identified as the most important factor, may be influenced by slight data variations. Overfitting countermeasures such as early stopping may improve, though a larger and more diverse dataset may be the only remedy. This indicates that the results obtained from ML should be critically analyzed.

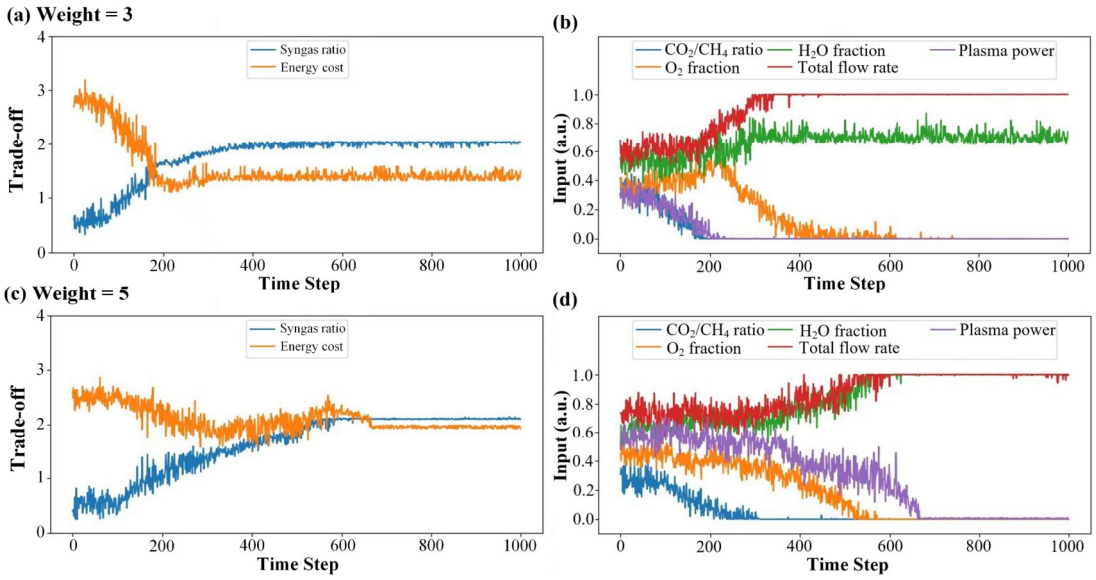

Fig. 9. Superposition of syngas ratio and energy cost, showing the best trade-offs (a, c), as well as the corresponding actions of the five input parameters (b, d), for different weights, i.e., relative importance of SR vs EC: weight = 3 (a) and (b), weight = 5 (c) and (d).

The ML results also require a comprehensive, human analysis towards practical application of APGD plasma reactors, based on prior knowledge. As mentioned before, the SR ideally reaches 2 for methanol production, which means that SR is our primary goal, rather than EC. Although the optimal results of the weighted superposition predicted by the RL model (i.e., SR of 1.88 with superior EC of 1.36 eV/molec, at SR/EC weight of 2) seems mathematically better than the best experimental data (SR of 2.03 and EC of 2.22 eV/molec), the predicted SR is still lower than 2, so it is not quite optimal for methanol production. We already know that the APGD is promising for its low EC, so we are willing to sacrifice the lower EC result to obtain a higher SR for application in methanol synthesis. To be competitive with other existing technologies producing syngas, Snoeckx and Bogaerts proposed a target value of 4.3 eV/(molec converted) (i.e., 412 kJ/mol) for plasma-based DRM (i.e., EC for conversion[11]), while we used EC for syngas production in our ML model development, allowing a more fair comparison between DRM, OCRM and BRM. Hence, if we transfer our result of EC (syngas) of 2.22 eV/molec to EC (conversion), which is 3.85 eV/molec (i.e., 369 kJ/mol), this value is still lower than the target of 4.3 eV/molec mentioned above. Hence, the best experimental data is suitable for the practical needs of further methanol production, because these conditions yield a SR of 2.03 and an EC below the proposed target. Our ML analysis predicts other conditions as optimal, because of the lower EC, but somewhat lower SR, hence not yet ideal for further methanol synthesis, probably because the defined weight (of SR vs EC) of 2 was not yet high enough.

Therefore, we also performed extra RL simulations with a higher weight (of SR vs EC) equal to 3 and 5, which lead to a higher maximum SR and minimum EC, as shown in Fig. 9, as expected. It is interesting to see that the RL simulations with (SR/EC) weight of 5 yield a maximum SR of 2.12 and a minimum EC of 2.04 eV/molec (i.e.,

352 kJ/mol), which is close to the best experimental results, at the same operating conditions (H_2O fraction of 45% and O_2 fraction of 0%). This illustrates it is possible to predict optimal values very close to the actual, experimental optimal data, and at the same experimental conditions, when selecting a suitable weight. Since we don't know in advance the exact weight needed to obtain the best SR in combination with EC, this illustrates that ML still needs human interpretation, when used over varying datasets.

4.4 ML model compared with other modelling methods

Compared to existing ML methods, this work developed a consistent ML method across different datasets (DRM, OCRM and BRM reactions), with high accuracy and adaptivity, achieving optimization on multi-performance metrics, as shown in Table 6.

Table 6. Comparison on the developed ML method and existing ML method.

Aspects	ML method used in this work	Existing ML method[32, 33]
Training dataset	Dataset from multiple reactions	Dataset from single reaction
Model type	Hybrid ML (SL +RL) method	SL method
Performance	Accurate ($R^2 > 0.96$)	Accurate ($R^2 > 0.98$)
Application	Static prediction + dynamic optimization	Static prediction
Outcome	Multi-objective optimization	Single-objective prediction

Table 7. Comparison on the developed data-driven ML models and mechanistic models.

Aspects	Data-driven ML models	Mechanistic models
Purpose	Real-time optimization and control	Revealing underlying mechanisms
Data needs	High (experimental data)	Low (input data limited to reactor geometry and operating conditions; everything else can be calculated)
Accuracy	High (within data domain)	High (with full physics and chemistry)
Computational cost	Low (available training data)	High (simulation time)
Interpretability	Low (black box)	High (insights in underlying mechanisms)

It should be realized that these ML methods do not provide mechanistic insights in the reaction kinetics and transport phenomena underlying the performance metrics. For this purpose, computational fluid dynamics and chemical kinetics models are needed. Such models have been developed in the past for the reactions under study. For instance, a quasi-one dimensional (quasi-1D) chemical kinetics model was developed to describe the plasma chemistry of DRM in the APGD plasma reactor studied in this work.[23] Furthermore, a sophisticated, fully coupled multi-dimensional model, consisting of a 2D axisymmetric plasma fluid dynamics model, a 3D gas flow model and a 0D detailed plasma chemistry model, was developed for OCRM in the APGD.[59] While a quasi-1D chemical kinetics model still needs to make assumptions on the gas flow in the plasma reactor, a fully coupled multi-dimensional model takes into account all relevant processes, including gas flow dynamics, plasma behavior, transport of species and plasma chemistry, and is therefore very powerful. It can even predict improved plasma reactor designs. Hence, these models can provide insights into the underlying physics

and chemistry, but on the other hand, they require significant computational resources and expertise. In Table 7 we compare the characteristics, strengths and limitations of our data-driven models with such mechanistic models.

4.5 ML applied to plasma-based gas conversion

Our SL method offers accurate prediction based on the dataset domain (i.e., the available data within the investigated range), but the RL results give somewhat different optimization when based on a single objective than the experiments. According to our RL model, the optimal EC can reach as low as 1 eV/molec when the CO_2/CH_4 ratio reaches 0.33, while the minimum EC in the current dataset was 1.26 eV/molec (i.e., 180 kJ/mol) when the CO_2/CH_4 ratio reaches 0.75 at the same O_2 fraction.

Ideally, the ML method is used to predict improved conditions based on limited experimental data, which are then tested experimentally, and indeed confirm that better results are reached at these new conditions. It should however be noted that such predicted conditions should fall within the dataset domain, to be more reliable. Indeed, the optimal value identified by the RL results would agree with the optimal experimental data if the RL model was trained on the dataset in the whole investigated range. However, it is much more difficult to cover a whole dataset when combining different reactions (i.e., DRM, OCRM and BRM), which explains the discrepancies between prediction and experimental results. For instance, the RL model results for EC prediction can be accurate within the dataset domain (i.e., CO_2/CH_4 ratio ranging from 0.75 to 1.9 in the presence of O_2). When the same model is employed to predict the values outside the dataset domain (CO_2/CH_4 ratio between 0.33 and 0.75 in the presence of O_2), the RL results based on the pattern learned within the dataset domain may not be reliable. Considering the CO_2/CH_4 ratio, O_2 fraction and H_2O fraction show near-linear trends toward the output variables within the dataset domain, which is consistent with that outside the dataset domain, our RL model results can still provide optimization policy (i.e., the regulation sequence on input parameters, as discussed in section 4.1) and qualitative analysis on experimental results based on the actions of agents. As the CO_2/CH_4 ratio is the negative factor for the EC, the optimal EC should be lower than the minimum value from the current dataset. Quantitative validation on the optimal results should be further tested by experiments.

ML is promising for prediction, within the dataset domain, but several challenges need to be addressed. As presented here, a sufficient amount of data across a broad range of testing conditions is required to ensure the robustness and relevance of the ML models. When comparing different reactions (although they are the same type), it is crucial to analyze their reaction performance in a consistent and fair manner. In addition, ML models cannot be used to explain the fundamental reaction mechanisms, so the interpretability of ML models can be limited, emphasizing the necessity of prior knowledge in evaluating ML results. As ML models are purely a data-driven method, they can only provide mathematically optimal results, but care should be taken to make smart decisions for practical application, as illustrated in previous section for the relative importance of SR vs EC (where SR might be more important for further methanol synthesis, if the EC is already acceptable).

Plasma-based gas conversion is a booming research field and more data are expected to become available in the coming years, which is important for enhancing the applicability of ML models. Indeed, it should be stressed that the size of the datasets needed to make ML useful and powerful is an open question to be investigated. Although combining various datasets extends the size of the dataset, it may impact the reliability of ML, while such imperfect dataset is indeed a realistic scenario in experimental data collection. On the other hand, hybrid algorithms are under investigation for developing accurate and reliable ML models, to be applied to various datasets. We believe this is a promising avenue for future ML research.

5. Conclusions

We developed a uniform, hybrid ML (SL and RL) model to predict and optimize plasma-based CO_2 and CH_4 conversion. The SL model utilizes a typical ANN algorithm for predicting reaction performance, reaching good agreement with the experimental data, indicated by R^2 values close to 1 for all output. The RL model for process optimization reveals that the optimal regulation policy on single output should prioritize coarse adjustments to high-impact parameters then fine-tuning low-impact ones. For the optimization of syngas ratio (SR) and energy cost (EC), our RL model reveals that the H_2O and O_2 fractions yield a trade-off between SR and EC. Furthermore, a CO_2/CH_4 ratio of 0.33, H_2O fraction of 45 % and no O_2 fraction result in a SR of 2.12 and EC (syngas) of 2.04 eV/molec (i.e., 352 kJ/mol), which is in close agreement with the best experimental data set (when optimized for SR of 2, towards methanol synthesis), demonstrating that the choice of weight (for SR vs EC) is very important. However, the optimal EC predicted by our RL models (around 1 eV/molec) is lower than the best experimental results, due to the different data domains across the DRM, OCRM and BRM reactions. Therefore, our ML model provides new insights to facilitate the optimization of intricate nonlinear and dynamic systems, like in plasma-based gas conversion.

Authorship contributions

Conceptualization, J.L. and A.B.; methodology & investigation, J.L., J. X. and B.W.; writing - original draft, J.L.; writing – review& editing, J.L., E.R. and A.B.; funding acquisition, J.L. and A.B., supervision, A.B.

Conflicts of interest

The authors declare that they have no known competing financial interests or personal relationships that could have appeared to influence the work reported in this paper.

Data availability

All data that support the findings of this study are included within the article (and any supplementary files).

Acknowledgments

This project received funding from the European Research Council (ERC) under the

European Union's Horizon 2020 research and innovation programme (grant agreement no.810182-SCOPE ERC Synergy project), and the University of Antwerp BOF-FWO postdoc seal of excellence mandate (grant agreement no.41/FA070200/FFB240228).

Reference

[1] D. Pakhare and J. Spivey, *Chem. Soc. Rev.*, 2014, **43**, 7813–7837.

[2] Y. Kathiraser, U. Oemar, E.T. Saw, Z. Li and S. Kawi, *Chem. Eng. J.*, 2015, **278**, 62–78.

[3] H. Zhao, R. Yu, S. Ma, K. Xu, Y. Chen, K. Jiang, Y. Fang, C. Zhu, X. Liu, Y. Tang, L. Wu, Y. Wu, Q. Jiang, P. He, Z. Liu and L. Tan, *Nat. Catal.*, 2022, **5**, 818–831.

[4] A.C. Vosloo, *Fuel Process. Technol.*, 2001, **71**, 149–155.

[5] O.-S. Joo, K.-D. Jung, I. Moon, A.Ya. Rozovskii, G.I. Lin, S.-H. Han and S.-J. Uhm, *Ind. Eng. Chem. Res.*, 1999, **38**, 1808–1812.

[6] I. Hannula, N. Kaisalo and P. Simell, *J. Carbon Res.*, 2020, **6**, 55.

[7] D. H. Chun, J. C. Park, S.Y. Hong, J. T. Lim, C. S. Kim, H.-T. Lee, J.-I. Yang, S. Hong and H. Jung, *J. Catal.*, 2014, **317**, 135–143.

[8] J. Slaets, M. Aghaei, S. Ceulemans, S.V. Alphen and A. Bogaerts, *Green Chem.*, 2020, **22**, 1366–1377.

[9] G. A. Olah, *Angew. Chem. Int. Ed.*, 2005, **44**, 2636–2639.

[10] A. A. Tountas, X. Peng, A. V. Tavasoli, P. N. Duchesne, T. L. Dingle, Y. Dong, L. Hurtado, A. Mohan, W. Sun, U. Ulmer, L. Wang, T. E. Wood, C. T. Maravelias, M. M. Sain and G. A. Ozin, *Adv. Sci.*, 2019, **6**, 1801903.

[11] R. Snoeckx and A. Bogaerts, *Chem. Soc. Rev.*, 2017, **46,** 5805–5863.

[12] H. Puliyalil, D. L. Jurković, V. D. B. C. Dasireddy and B. Likozar, *RSC Adv.*, 2018, **8,** 27481–27508

[13] A. George, B. Shen, M. Craven, Y. Wang, D. Kang, C. Wu and X. Tu, *Renew. Sust. Energ. Rev.*, 2021, **135**, 109702.

[14] J. Osorio-Tejada, M. Escriba-Gelonch, R. Vertongen, A. Bogaerts and V. Hessel, *Energy Environ. Sci.*, 2024, **17**, 5833–5853.

[15] F. Zhang, X. Zhang, Z. Song, X. Li, X. Zhao, J. Sun, Y. Mao, X. Wang and W. Wang, *Fuel*, 2023, **331**, 125914.

[16] R. B. Raja, A. C. Halageri, R. Sankar, R. Sarathi and R. Vinu, *Energies,* 2023, **16**, 1823.

[17] J. A. Andersen, J. M. Christensen, M. Østberg, A. Bogaerts and A.D. Jensen, *Chem. Eng. J.*, 2020, **397**, 125519.

[18] K. Li, J.-L. Liu, X.-S. Li, X. Zhu and A.-M. Zhu, Chem. Eng. J., 2016, 288, 671–679.

[19] O. Biondo, C.F.A.M. van Deursen, A. Hughes, A. van de Steeg, W. Bongers, M.C.M. van de Sanden, G. van Rooij and A. Bogaerts, *Green Chem.*, 2023, **25**, 10485–10497.

[20] Y. Diao, H. Wang, B. Chen, X. Zhang and C. Shi, *Appl. Catal. B: Environ.*, 2023, **330**, 122573.

[21] J. L. Liu, X. Wang, X. S. Li, B. Likozar and A. M. Zhu, *J. Phys. D: Appl. Phys.*, 2020, **53**, 253001.

[22] D. L. Jurković, J. L. Liu, A. Pohara and B. Likozar, *Catal. Today*, 2021, **362,** 11-21.

[23] B. Wanten, S. Maerivoet, C. Vantomme, J. Slaets, G. Trenchev and A. Bogaerts, *J. CO2 Util.*, 2022, **56**, 101869.

[24] S. Maerivoet, B. Wanten, R. De Meyer, M. Van Hove, S. Van Alphen and A. Bogaerts, *ACS Sustain. Chem. Eng.*, 2024, **12**, 11419−11434.

[25] G. Ni, Y. Lan, C. Cheng, Y. Meng and X. Wang, *Int. J. Hydrogen Energ.*, 2011, **36**, 12869–12876.
[26] B. Wanten, Y. Gorbanev and A. Bogaerts, *Fuel*, 2024, **374**, 132355.
[27] T. Toyao, Z. Maeno, S. Takakusagi, T. Kamachi, I. Takigawa and K. Shimizu, *ACS Catal.*, 2020, **10**, 2260–2297.
[28] M. Witman, D. Gidon, D. B. Graves, B. Smit and A. Mesbah, *Plasma Sources Sci. Technol.*, 2019, **28**, 095019.
[29] A. D. Bonzanini, K. Shao, D. B. Graves, S. Hamaguchi and A. Mesbah, *Plasma Sources Sci. Technol.*, 2023, **32**, 024003.
[30] U.K. Ercan, G.D. Özdemir, M.A. Özdemir and O. Güren, *Plasma Process. Polym.*, 2023, **20**, e2300066.
[31] M. Suvarna, T.P. Araújo and J. Pérez-Ramírez, *Appl. Catal. B: Environ.*, 2022, **315**, 121530.
[32] A. Bhardwaj, A. S. Ahluwalia, K. K. Pant and S. Upadhyayula, *Sep. Purif. Technol.*, 2023, **324**, 124576.
[33] S. Kumar, G. Ignacz and G. Szekely, *Green Chem.*, 2021, **23,** 8932–8939.
[34] Y. Kim, J. Cho, H. Jung, L. E. Meyer, G. M. Fioroni, C. D. Stubbs, K. Jeong, R. L. McCormick, P. C. John and S. Kim, *Green Chem.*, 2024, **26,** 10247–10264.
[35] G. Ignacz, A. K. Beke, V. Toth and G. Szekely, *Nat. Energy*, 2024.
[36] S. Y. Liu, D. H. Mei, Z. Shen and X. Tu, *J. Phys. Chem. C*, 2014, **118**, 10686–10693.
[37] X. Zhu, S. Liu, Y. Cai, X. Gao, J. Zhou, C. Zheng and X. Tu, *Appl. Catal. B: Environ.*, 2016, **183**, 124–132.
[38] Y. Wang, Y. Chen, J. Harding, H. He, A. Bogaerts and X. Tu, *Chem. Eng. J.*, 2022, **450**, 137860.
[39] Y. Cai, D. Mei, Y. Chen, A. Bogaerts and X. Tu, *J. Energ. Chem.*, 2024, **96**, 153–163.
[40] J. Li, J. Xu, E. Rebrov and A. Bogaerts, *Chem. Eng. J.*, 2025, **507**, 159897.
[41] B. Ashford, Y. Wang, C.-K. Poh, L. Chen and X. Tu, *Appl. Catal. B: Environ.*, 2020, **276**, 119110.
[42] D. Mei, B. Ashford, Y.-L. He and X. Tu, *Plasma Process. Polym.*, 2017, **14**, 1600076.
[43] J.-S. Kim, I. Chung, J. Oh, J. Park, Y. Yun, J. Shin, H.W. Kim and H. Chang, *J. CO2 Util.*, 2023, **78**, 102620.
[44] X. Wang, X. Du, K. Chen, Z. Zheng, Y. Liu, X. Shen and C. Hu, *ACS Sustain. Chem. Eng.*, 2023, **11**, 4543–4554.
[45] J. Li, L. Pan, M. Suvarna and X. Wang, *Chem. Eng. J.*, 2021, **426**, 131285.
[46] Y. Shen, C. Fu, W. Luo, Z. Liang, Z.-R. Wang and Q. Huang, *Green Chem.*, 2023, **25**, 7605–7611.
[47] D. Tan, M. Suvarna, Y. Shee Tan, J. Li and X. Wang, *Appl. Energ.*, 2021, **291**, 116808.
[48] X. Yuan, M. Suvarna, S. Low, P. D. Dissanayake, K. B. Lee, J. Li, X. Wang and Y.S. Ok, *Environ. Sci. Technol.*, 2021, **55**, 11925–11936.
[49] Y. Gao, Z. Saedi, H. Shi, B. Zeng, B. Zhang and X. Zhang, *ACS EST Water*, 2024, **4**, 735–750.
[50] R.S. Sutton and A.G. Barto, Cambridge, MA, USA: 624 MIT Press (2018).
[51] J. Schulman, F. Wolski, P. Dhariwal, A. Radford and O. Klimov, (2017).
[52] K. Wang, H. Zhang, A. J, L. Rao, X. Lin, J. Wan, Y. Long, M. Gao, W. Wang, X. Tu, X. Li and Q. Huang, *Fuel Process. Technol.*, 2023, **248**, 107826.
[53] U.S. Mohanty, M. Ali, M.R. Azhar, A. Al-Yaseri, A. Keshavarz and S. Iglauer, *Int. J. Hydrogen Energ.*, 2021, **46**, 32809–32845.

[54] D. Czylkowski, B. Hrycak, M. Jasiński, M. Dors and J. Mizeraczyk, *Energy*, 2016, **113**, 653–661.
[55] Y. Xia, N. Lu, J. Li, N. Jiang, K. Shang and Y. Wu, *J. CO2 Util.*, 2020, **37**, 248–259.
[56] X. Zhao, B. Joseph, J. Kuhn and S. Ozcan, *iScience*, 2020, **23**, 101082.
[57] B. Hrycak, J. Mizeraczyk, D. Czylkowski, M. Dors, M. Budnarowska and M. Jasiński, *Sci. Rep.*, 2023, **13**, 2204.
[58] T. Yabe and Y. Sekine, *Fuel Process. Technol.*, 2018, **181**, 187–198.
[59] S. Maerivoet, I. Tsonev, J. Slaets, F. Reniers and A. Bogaerts, *Chem. Eng. J.*, 2024, **492**, 152006.